ISTITUTO NAZIONALE DI FISICA NUCLEARE

Sezione di Genova

INFN/BE-95/03
3 Marzo 1995

M. Taiuti , V.I. Mokeev, M. Anghinolfi, N. Bianchi, G.P. Capitani, P. Corvisiero, E. DeSanctis, P. Levi Sandri, V. Muccifora, M. Olcese, E. Polli, G. Ricco, A.R. Reolon, M. Ripani, P. Rossi, M. Sanzone, A. Zucchiatti:

THE LARGE ANGLE ELECTROMAGNETIC SHOWER CALORIMETER FOR CLAS: MODULE DESIGN AND OPTIMISATION OF PERFORMANCIES

SIS-Pubblicazioni
dei Laboratori Nazionali di Frascati

INFN - Istituto Nazionale di Fisica Nucleare
Sezione di Genova

INFN/BE-95/03
3 Marzo 1995

THE LARGE ANGLE ELECTROMAGNETIC SHOWER CALORIMETER FOR CLAS: MODULE DESIGN AND OPTIMISATION OF PERFORMANCIES

M. Taiuti[1], V.I. Mokeev[2], M. Anghinolfi[1], N. Bianchi[3], G.P. Capitani[3], P. Corvisiero[1], E. DeSanctis[3], P. Levi Sandri[3], V. Muccifora[3], M. Olcese[1], E. Polli[3], G. Ricco[1], A.R. Reolon[3], M. Ripani[1], P. Rossi[3], M. Sanzone[1], A. Zucchiatti[1]

1) Dipartimento di Fisica dell'Università di Genova or I.N.F.N.-Sezione di Genova, I-16146, Genova, Italy.
2) Institute of Nuclear Physics, Moscow State University.
3) I.N.F.N.-Laboratori Nazionali di Frascati, P.O.Box 13, I-00044, Frascati , Italy.

Abstract

The AIACE collaboration is realizing modules of the Large Angle Electromagnetic Shower Calorimeter for CLAS. The module internal structure has been designed using Monte Carlo simulations to provide the best response to electron-pion separation, photon and neutron detection considering all the kinematics and mechanical constraints provided by CLAS. We found out that it was possible first to optimise the intrinsic response function and then to study the effect of light collection on the best obtained response. To optimise the response function we introduced a factor of merit F comprehensive of the most important parameters.

1. - INTRODUCTION

The AIACE collaboration[1] participates to the CEBAF[2] Hall B experimental activity and will provide modules of the Electromagnetic Shower Calorimeter (AIACE-ESC) to detect particles at angle larger than 45° in the laboratory. The CEBAF Hall B is equipped with a Large Acceptance Spectrometer (CLAS) based on a toroidal field generated by six superconducting coils arranged around the beam line[3]. The detecting system consists of Drift Chambers to reconstruct the track of charged particles, Threshold Gas Cherenkov Counters for electron identification, Scintillation Counters for the trigger and for time-of-flight measurements, and an Electromagnetic Shower Calorimeter (ESC). The segments are individually instrumented to form six independent magnetic spectrometers. This will help pattern recognition and track reconstruction at high luminosity.

The Cherenkov Counters are sensitive to particles with $\beta \geq 0.998$. In combination with the ESC they give good electron identification, sufficient even at large electron scattering angles were the π/e ratio become large.

The ESC is used for a) the π/e separation, b) the detection of photons from the decay of mesons (π^0, η, η' ...) and baryons (Λ^* ...) and c) the measurement of neutron momentum using time-of-flight. The last requirement suggested to study the same materials adopted for the forward ESC, that is lead sheets and plastic scintillator bars arranged in a multi-layers configuration.

The electron and photon energy range is 0.0 ÷ 2.0 GeV being defined by the most energetic electron scattered at angles higher than 45° from a 6 GeV electron beam.

The ESC performances are very sensitive a) to its internal structure (like the lead and plastic scintillator thickness and number of layers) and b) to the efficiency of light collection (like light attenuation in scintillators and the number of collected photo-electrons). We studied the effect of each parameter by means of a Monte Carlo simulation program based on the GEANT 3.14[4] package.

We found that in order to design the calorimeter it was possible to estimate first the effect of the module structure on the intrinsic response function and then to study the effect of light collection on the best obtained response. We present in this paper the result of the optimisation of the intrinsic response function leaving to a second report the discussion of the light collection contributions.

2. - THE AIACE-ESC MODULE - GENERAL DESCRIPTION

Each AIACE-ESC module is based on a multi-layer structure made by lead sheets and scintillator bars, like the forward ESC. There are 33 layers, each composed by a lead foil with

thickness 0.20 cm and plastic scintillator bars with average width 10 cm and constant thickness 1.5 cm. Consecutive layers are placed at 90° to form a 40x24 matrix of 10x10 cm^2 cells. In table 1 dimensions of all scintillators are reported as a function of the layer number; the width increases going from the inner side toward the outer to guarantee the tapering required by the CLAS geometry. The surface exposed to particle fluxes is 216.9x400.1 cm^2.

short scintillators				long scintillators			
layer	length	width	amount	layer	length	width	amount
1	216.9	10.03	40	2	402.7	9.10	24
3	218.4	10.10	40	4	405.5	9.16	24
5	219.9	10.17	40	6	408.3	9.22	24
7	221.4	10.24	40	8	411.1	9.28	24
9	222.9	10.31	40	10	413.9	9.34	24
11	224.4	10.38	40	12	416.7	9.40	24
13	225.9	10.45	40	14	419.5	9.46	24
15	227.4	10.52	40	16	422.3	9.52	24
17	228.9	10.59	40	18	425.1	9.58	24
19	230.4	10.66	40	20	427.9	9.64	24
21	231.9	10.73	40	22	430.7	9.70	24
23	233.4	10.80	40	24	433.5	9.76	24
25	234.9	10.87	40	26	436.3	9.82	24
27	236.4	10.94	40	28	439.1	9.88	24
29	237.9	11.01	40	30	441.9	9.94	24
31	239.4	11.08	40	32	444.7	10.00	24
33	240.9	11.15	40				

Table 1 - Dimensions and quantity of scintillator bars for one AIACE-ESC module.

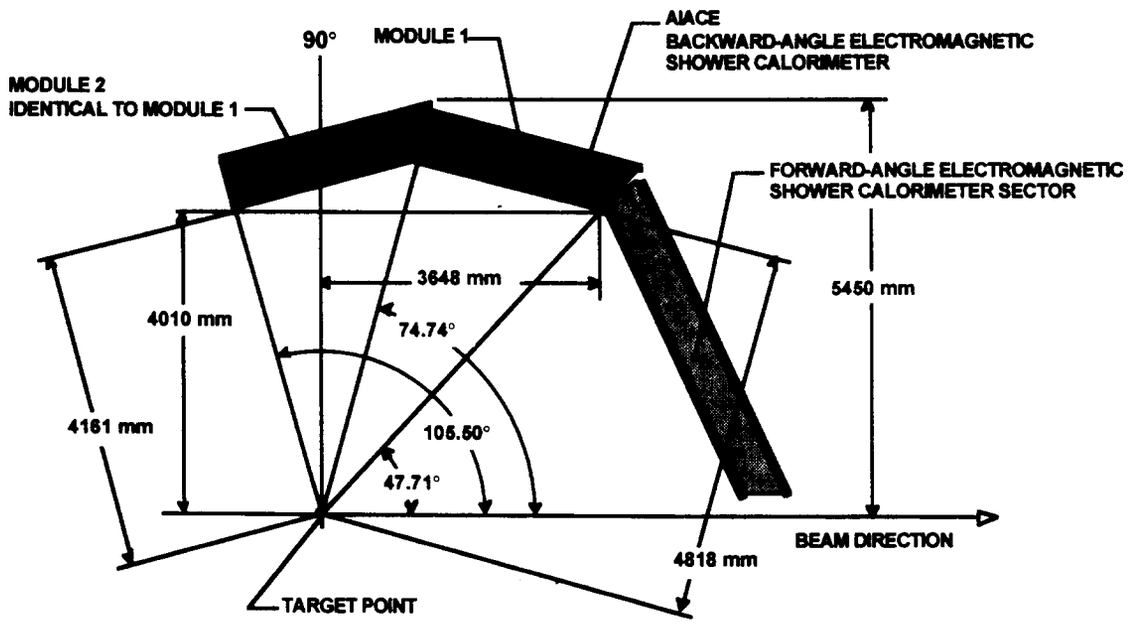

Figure 1 - Conceptual design of the ESC-AIACE modules shown together with a forward-angle ESC module.

The module is longitudinally divided, with respect to the incoming particle direction, into an inner and an outer part to improve the electron-pion discrimination. Scintillators lying (for the inner and outer part separately) one on top of the other with the same orientation form 128 different stacks.

The electromagnetic showers originate in the lead sheets and propagate through the module; the fraction absorbed in the active material produces a light pulse that is collected at both scintillator ends. The collected light is summed, separately for each stack, using light guides before the photomultiplier. The AIACE-ESC modules are the most external structure of the CLAS detector and the limitations given by the Hall B ground floor and crane set the maximum thickness to 60 cm. The external shape was optimised to reduce dead volumes: in fig.1 we show how it is possible to cover θ range from a few degrees up to $\approx 105°$ using one forward ESC module and two AIACE-ESC modules.

3. - THE INTRINSIC RESPONSE FUNCTION

The calorimeter performs three different tasks and each task requires a priori a different module structure. During the module design we had to consider this and we tried to find the configuration that provides the best compromise. We focused ourselves on a) the energy resolution σ_E/E, b) the radiation and absorption lengths ratio L_{rad}/L_{abs}, c) the total plastic scintillator thickness $X_{pl.sc.}$ and d) the number of layers N representing the module complexity.

The effect of each parameter is discussed in more detail in the following sections while in table 2 the results are summarised for all studied configurations as a factor of merit F defined as

$$F = \frac{L_{rad}/L_{abs}\, X_{pl.sc.}}{N \left.\frac{\sigma_E}{E}\right|_{(E=0.5GeV)}} \qquad 1)$$

where the energy resolution for photon uniformly emitted from a point source placed in the focus of the module has been evaluated at the energy of 0.5 GeV because the simulations showed that at this energy the calorimeter energy resolution is more sensitive to the internal structure. Therefore the factor F permitted to select the three most promising configurations outlined in table 2 and a more detailed analysis based on the energy dependence of σ_E/E showed that the adopted configuration provides the best energy resolution in the whole energy range.

lead thickness (cm)	plastic scintillator thickness (cm)	N	σ_E/E (%) (E = 0.5 GeV)	total thickness (cm)	$X_{pl.sc.}$ (cm)	L_{rad}	L_{abs}	L_{rad}/L_{abs}	F
0.05	1.0	57	12.24	59.85	57	6.42	0.88	7.3	0.59
0.05	1.5	38	21.92	58.9	57	4.73	0.83	5.7	0.39
0.10	1.0	39	10.81	42.9	39	7.87	0.72	10.9	1.01
0.10	1.0	42	10.01	46.2	42	8.47	0.77	10.9	1.09
0.10	1.0	48	7.91	52.8	48	9.68	0.88	10.9	1.38
0.10	1.0	54	7.62	59.4	54	10.89	1.00	10.9	1.44
0.10	1.5	37	8.20	59.2	55.5	7.90	0.91	8.6	1.58
0.10	2.0	28	12.60	58.8	56	6.31	0.87	7.3	1.15
0.15	1.0	39	9.60	44.85	39	11.34	0.83	13.6	1.42
0.15	1.0	52	8.74	59.8	52	15.12	1.11	13.6	1.56
0.15	1.5	30	9.05	49.5	45	9.08	0.83	10.9	1.81
0.15	1.5	33	8.80	54.45	49.5	9.99	0.91	10.9	1.87
0.15	1.5	36	8.63	59.4	54	10.89	1.00	10.9	1.90
0.15	2.0	27	10.32	58.05	54	8.49	0.92	9.3	1.79
0.20	1.0	30	11.16	36	30	11.40	0.73	15.6	1.40
0.20	1.0	33	10.96	39.6	33	12.54	0.80	15.6	1.43
0.20	1.0	36	10.63	43.2	36	13.68	0.87	15.6	1.47
0.20	1.0	39	10.06	46.8	39	14.82	0.95	15.6	1.56
0.20	1.0	50	9.01	60	50	19.00	1.21	15.6	1.74
0.20	1.5	30	9.83	51	45	11.75	0.92	12.8	1.95
0.20	**1.5**	**33**	**9.16**	**56.1**	**49.5**	**12.93**	**1.01**	**12.8**	**2.10**
0.20	1.5	35	9.45	59.5	52.5	13.71	1.07	12.8	2.03
0.20	**2.0**	**27**	**9.82**	**59.4**	**54**	**10.89**	**1.00**	**10.9**	**2.23**
0.25	1.0	39	11.59	48.75	39	18.29	1.06	17.2	1.49
0.25	1.0	48	11.50	60	48	22.51	1.31	17.2	1.50
0.25	**1.5**	**34**	**10.08**	**59.5**	**51**	**16.35**	**1.14**	**14.4**	**2.14**
0.30	1.0	39	12.39	50.7	39	21.77	1.18	18.5	1.49
0.40	1.0	39	16.08	54.6	39	28.71	1.40	20.5	1.27

Table 2 - Quality factor F for different AIACE-ESC module configurations. The configurations corresponding to the best F values are outlined.

3.1 - The π^0 and η mass reconstruction

The neutral particle mass reconstruction is strongly affected by the error on the energy and relative angle of the decay photons. The mass value m and resolution σ_m are defined by the following equations

$$m^2 = 2E_1E_2(1-\cos\theta) \qquad 2)$$

$$\left(\frac{\sigma_m}{m}\right)^2 = \left(\frac{\sigma_{E_1}}{2E_1}\right)^2 + \left(\frac{\sigma_{E_2}}{2E_2}\right)^2 + \left(\frac{\sigma_{\cos\theta}}{2(1-\cos\theta)}\right)^2 \qquad 3)$$

where E and σ_E are the photon energy and energy resolution while θ and σ_θ are the relative angle and its resolution. The total energy E is obtained summing the deposited energy over 5 stacks as follows:

$$E = \sum_{i=-2}^{2} E_i \qquad 4)$$

and the cosθ value can be obtained from the electromagnetic shower radial centroid averaging the stack coordinates with the deposited energy as follows

$$x = \sum_{i=-2}^{2} x_i E_i \Big/ \sum_{i=-2}^{2} E_i \qquad 5)$$

being i=0 the coordinate of the stack corresponding to the maximum deposited energy. In fig.2 the expected position reconstruction for photons from decay of π^0 with 1.0 GeV/c momentum, uniformly emitted from a point source 5 meter far from the AIACE-ESC module, is reported: the resolution σ_x is approximately 2.5 cm and $\sigma_{\cos\theta} = 0.9\ 10^{-4}$.

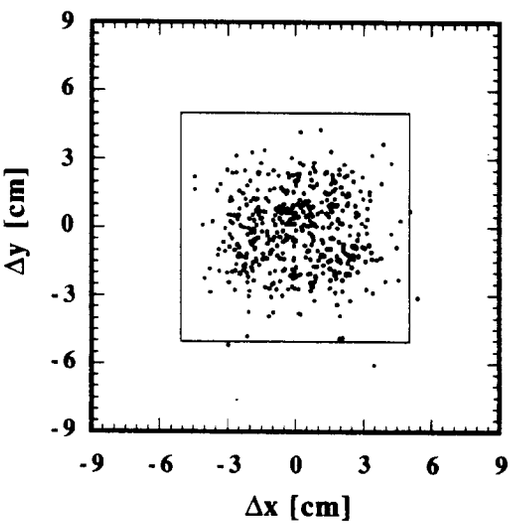

Figure 2 - Position reconstruction for photons from the decay of 1 GeV/c π^0 uniformly emitted from a point source 5 meter apart from the AIACE-ESC module. The square represents the cell dimensions.

In fig.3 the contribution of energy and angle resolution are shown for π^0 and η as a function of the particle momentum for the most probable decay in the laboratory frame $E_1 = E_2$ and with the deposited energy and angular resolutions obtained from the simulations. The main contribution is given by the energy resolution that dominates in the η mass reconstruction even at momentum values as high as 4 GeV/c and in the π^0 mass reconstruction up to 1 GeV/c. Only at higher momentum, where the θ most probable value becomes lower than 10°, the angular resolution dominates.

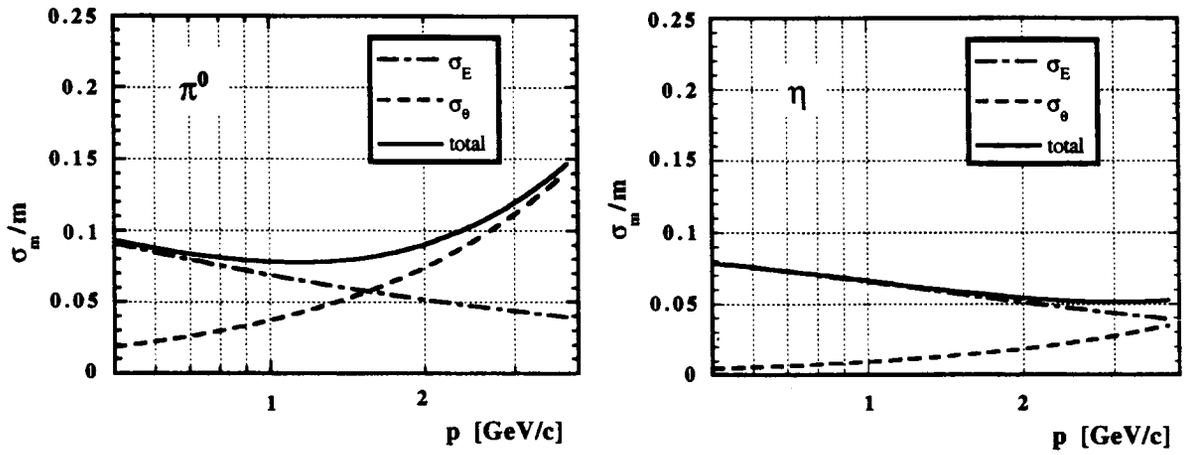

Figure 3 - Mass reconstruction resolution for π^0 (left) and η (right) as a function of the particle momentum showing the contribution of energy resolution (dash-dotted line) and angular resolution (dashed line).

Therefore we studied separately the effect of scintillator and lead thickness on deposited energy in the active part of the module and energy resolution. We combined plastic layers with thickness equal to 1.0 or 1.5 cm (higher values are less efficient due to the constraints on the module total thickness) and lead sheets with thickness 0.10, 0.15 or 0.20 cm. The number of layer ranged in such a way that the module thickness was lower than 60 cm. We studied the module response function simulating 0.1, 0.5, 1.0 and 2.0 GeV electron beams emitted from a point source 5 meter far from the module and impinging uniformly on the inner surface. The response function is generally gaussian with a low energy tail due to energy leakage from lateral surfaces. We did not extend the simulations at higher values of the plastic scintillator thickness because the energy resolution is too low already at 1.0 GeV. In fig.4 the simulation results are reported for deposited energy E_d and resolution σ_E/E for electron beams with kinetic energy 0.5 GeV; the final configuration is indicated with a black arrow. Analytically the deposited energy and energy resolution behaviours are

$$E_d = (364.7 \pm 1.2)E \qquad \text{[MeV]} \qquad 6)$$

$$\frac{\sigma_E}{E} = (6.4 \pm 0.2)E^{-(0.47 \pm 0.02)} \qquad [\%] \qquad 7)$$

with E in GeV. The power law, very close to $\sqrt{E}$, confirms that the chosen internal structure is suitable to contain the electromagnetic shower up to 2 GeV without appreciable energy leakage.

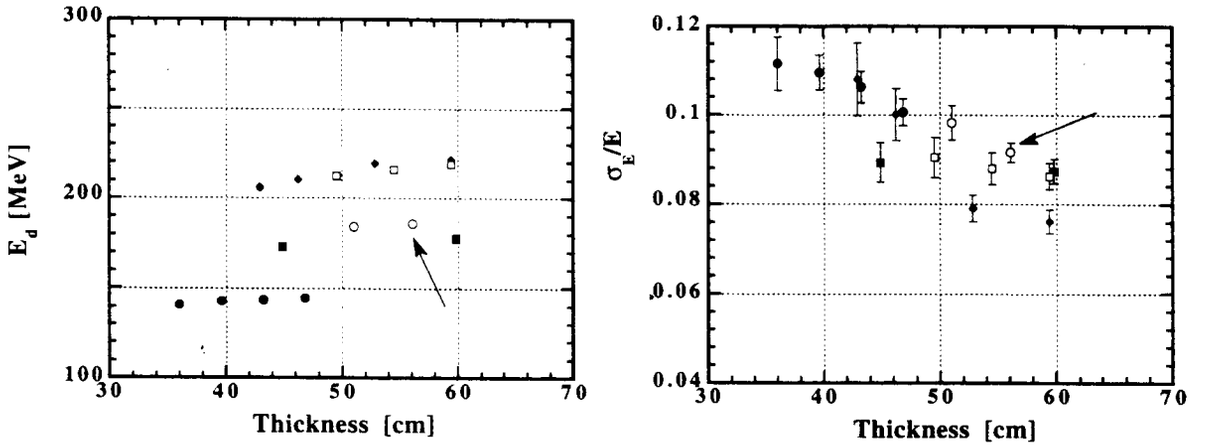

Figure 4 - Deposited energy (left) and energy resolution (right) for 0.5 GeV electrons that uniformly irradiate the front surface plotted as a function of the AIACE-ESC thickness and for different AIACE-ESC configurations: plastic thickness of 1.0 cm (full points), 1.5 cm (empty points), lead thickness of 0.10 cm (diamonds), 0.15 cm (squares) and 0.20 cm (circles). The black arrow shows the final configuration.

3.2 - The electron-pion separation

In fig.5 the deposited energy for 2 GeV/c electrons and pions is reported. Most of the incoming pions loose energy only by ionisation and can be easily rejected with a suitable energy threshold. A non negligible fraction of incoming pions, however, inelastically interacts with the calorimeter, originating through exchange charge mechanisms like (π^-, π^0) a secondary electromagnetic shower that strongly increases the pion deposited energy.

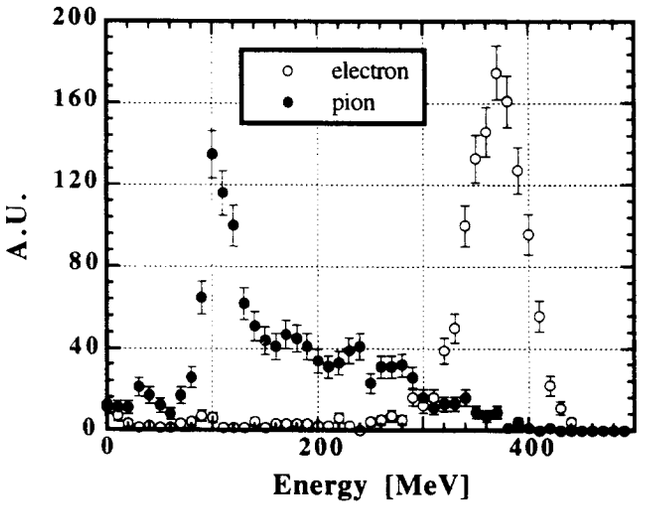

Figure 5 - Deposited energy by 2.0 GeV/c electrons (empty dots) and pions (full dots) that uniformly irradiate the front surface.

This effect becomes comparable to the energy released by electrons with same momentum. To minimise this effect the ratio L_{rad}/L_{abs} and the energy resolution have to be maximised.

To improve the pion rejection the analysis of the longitudinal and transversal shape of the shower has to be performed. In fig.6 the average deposited energy in each layer for 1 GeV/c electrons and pions is reported. In order to maximise the deposited energy difference we chose to assign 16 layers to the inner part and 17 to the outer.

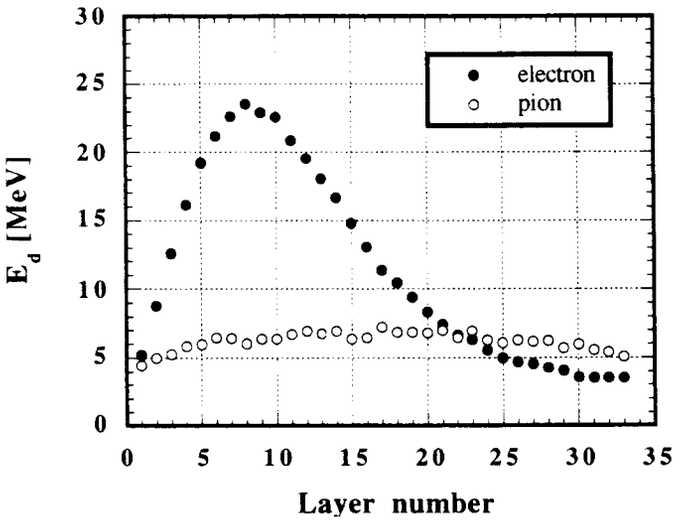

Figure 6 - Mean deposited energy in each module layer by 1.0 GeV/c electrons (full dots) and pions (empty dots) that uniformly irradiate the front surface.

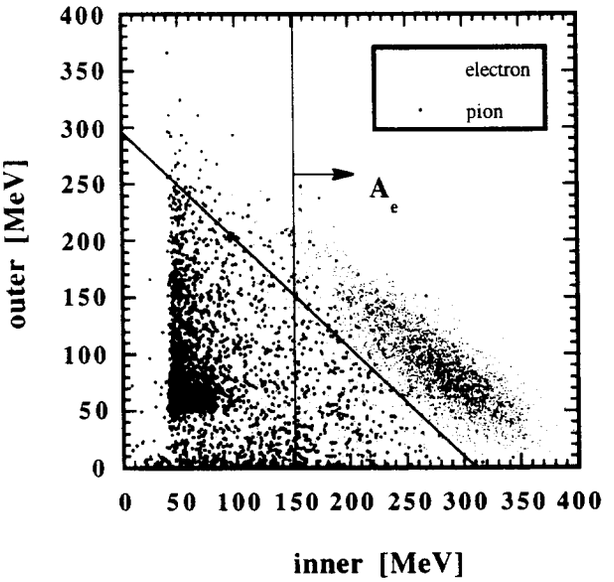

Figure 7 - Deposited energy in the outer part of the module for 1 GeV/c momentum electron (light dots) and pion (heavy dots) vs. deposited energy in the inner part.

The energy released by electrons in the inner part of the module is typically three times higher than that released by pions with same momentum. This division will also permit to equally distribute the scintillator among the collecting light systems. To discriminate electrons from pions with same momentum we investigated a three step procedure. First the region A_e corresponding to 92% of electron is selected as shown in fig.7 where the deposited energy in outer part vs. the deposited energy in the inner part of the module is plotted for 1 GeV/c momentum electrons and pions; then the deviation of the centroid of the shower from the particle incoming direction is analysed using expression 4). Finally the shower transverse radius is evaluated.

The efficiency is described by two functions of the particle momentum: a) the rejection R and b) the confusion C defined as

$$R = \frac{\pi_{out}}{\pi_{in}} \qquad \text{and} \qquad C = \frac{\pi_{in}}{e_{in} + \pi_{in}} \qquad 8)$$

being π_{out} the number of pion outside region A_e, π_{in} the number of pion inside region A_e and e_i the number of pion inside region A_e. In fig.8 the momentum dependence of R and C is reported.

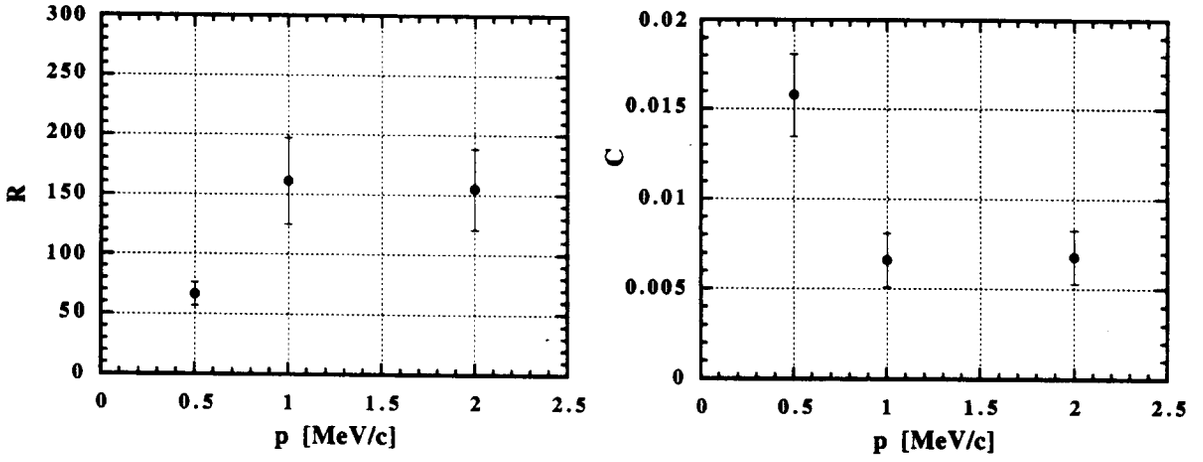

Figure 8 - Rejection factor R (left) and confusion factor C (right) as a function of the incoming particle momentum.

We also evaluated the maximum deposited energy in one stack separately for the inner and outer part corresponding to 2 GeV/c electrons. The results, reported in fig.9, show that electrons can release in the inner part all the energy they release in the active part of the calorimeter while the deposited energy in the outer part is lower than 250 MeV. These distributions, convoluted with the efficiency of the collecting light system, will affect the reconstruction of the e.m. shower shape and the neutron detection efficiency.

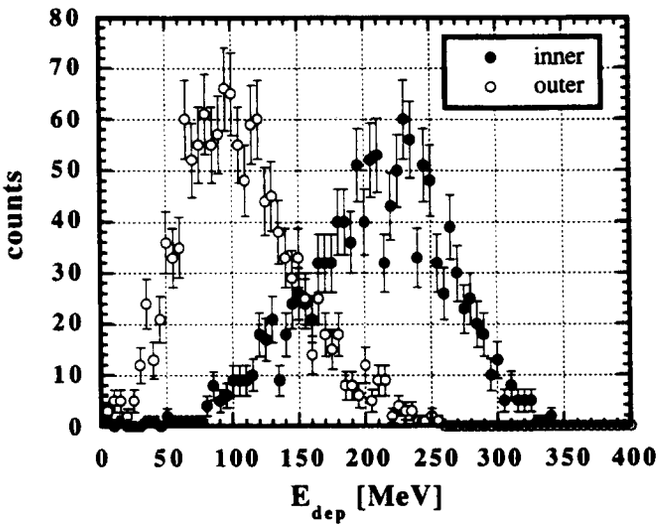

Figure 9 - Deposited energy in a single stack for 2 GeV/c electrons in the inner part (full dots) and outer part (empty dots) of the module.

3.3 - The neutron detection

The neutron momentum is evaluated measuring the length of the trajectory L from the target to the first interaction point in the calorimeter and the elapsed time τ. Analytically the reconstructed momentum resolution is related to length and time uncertainties σ_L and σ_τ by the relation

$$\frac{\sigma_p}{p} = \frac{\left(\sigma_L^2 + v_n^2 \sigma_\tau^2\right)^{1/2}}{\left(1 - v_n^2 / c^2\right) L} \qquad 9)$$

where v_n is the neutron velocity. The length resolution σ_L depends on the precision of the coordinates of the first interaction point. This effect can be evaluated observing that, since the module is approximately 500 cm far from the target, the main contribution to σ_L arises from the longitudinal coordinate z. The probability that a neutron interacts in the calorimeter does not depend on the interaction point depth and, because the module thickness is equal to one nuclear absorption length, the interaction point probability function can be well approximated with a step function with 56 cm full width and the second order momentum σ_z equal to $\sqrt{3}/6$ times the module thickness. The inner-outer subdivision reduces this uncertainties by a factor of two providing the full width value 28 cm and a σ_L value equal to 8 cm. The time resolution σ_τ depends, on the contrary, on a) the z coordinate, b) the light propagation properties in scintillators and light guides and c) on time fluctuations in photomultipliers. The first contribution for 1 GeV/c neutron momentum is $\sigma_\tau \approx 200$ psec or $v_n \sigma_\tau \approx 9$ cm but can be

improved using light guides with different length for each scintillator. This will reduce the light path to the photomultiplier for farther scintillators and increase it for closer scintillators. Contributions b) and c) strongly depend on the experimental configuration and cannot be discussed in this paper. However we can conclude that it is highly desirable that these contributions would be at least comparable to σ_z .

4. - CONCLUSIONS

We studied the intrinsic response function of the AIACE Electromagnetic Shower Calorimeter that will be installed in CLAS for detection of scattered electrons, photons and neutrons emitted at angles larger than 45° in the laboratory frame. Each module has a rectangular shape and an internal structure similar to that of the Forward ESC. Its active surface is 216.9x400.1 cm^2, it covers an azimuth angle interval of 25°. To select the best configuration we introduced a factor of merit F comprehensive of the most important parameters. We found that the best module is composed by 33 lead/scintillator layers; each layers being realised with a lead foil 0.2 cm thick and plastic scintillator bars 1.5 cm thick with average width 10 cm. Each scintillator layer is rotated of 90° to form ≈ 10x10 cm^2 cells. The module is divided, along the incoming particle trajectory, into two parts to improve electron-pion discrimination. The detector thickness is 12.86 radiation length or 0.99 absorption length.

The linear energy range is 0.0 ÷ 2.0 GeV and the intrinsic energy resolution is $\frac{\sigma_E}{E} = 6.4E^{-0.47}$ [%] with E in GeV. However, to obtain a realistic response function the contribution of collected light has to be evaluated.

Up to 12 modules can be installed in CLAS to detect particle emitted ad θ angles from 50° to 105°.

ACKNOWLEDGEMENT

We would like to thank V.Burkert (CEBAF) for the fruitful discussions on the calorimeter simulation results.

REFERENCES

(1) J.J.Domingo, Proceedings of the *5th Workshop on Perspectives in Nuclear Physics at Intermediate Energies*, Trieste May 6-10, 1991, ed. by S.Boffi, C.Ciofi degli Atti and M.Giannini, World Scientific (1992) p.260.

(2) M.Anghinolfi et al., Proceedings of the *International Workshop on Flavour and Spin in Hadronic and Electromagnetic Interactions*, Torino September 21-23, 1992, ed. by F.Balestra, R.Bertini and R.Garfagnini, Italian Physical Society vol.39 (1993) p.237.

(3) Conceptual Design Report - Basic Experimental Equipment, CEBAF April 13, 1990.

(4) R.Brun, F.Bruyant, M.Maire, A.C.McPherson and P.Zanarini, GEANT3 User Guide, CERN/DD/EE/84-1 (1987).